Optimal variable stiffness distribution for a composite plate with a row of holes subjected to tension/shear load cases

Conference Paper · June 2015

DOI: 10.2514/6.2015-2488

CITATIONS
5

READS
95

4 authors:

Michael Van tooren
University of South Carolina
242 PUBLICATIONS **2,456** CITATIONS
SEE PROFILE

Ali Elham
Technische Universität Braunschweig
68 PUBLICATIONS **343** CITATIONS
SEE PROFILE

Ramy Harik
University of South Carolina
91 PUBLICATIONS **1,001** CITATIONS
SEE PROFILE

Ahsan Uddin
University of South Carolina
8 PUBLICATIONS **30** CITATIONS
SEE PROFILE

Optimal variable stiffness distribution for a composite plate with a row of holes subjected to tension/shear load cases

Michel.J.L. van Tooren*
University of South Carolina, Columbia, SC, 29201

Ali Elham†
Delft University of Technology, 2629HS Delft, The Netherlands

Ramy Harik‡ and Ahsan Uddin§
University of South Carolina, Columbia, SC, 29201

This paper presents a framework for the design of variable stiffness fiber composite panels subject to multiple load cases, each case a combination of tension and shear. The framework consists of a finite element (FE) solver, an optimizer, a module that controls the link between design variables and the stiffness matrix in the FE module, and a post-processor that translates the theoretical optimal result from the optimizer into discrete tow paths for each ply. The dual mesh formulation of the design variables using a manufacturing mesh separate from the FE mesh limits the number of design variables while preserving smoothness and allows easy specification of manufacturing constraints enforced by the envisioned fiber steering process, for example the minimum course radius to prevent tow buckling. It also allows the incorporation of constraints related to fusion bonding techniques for continuous carbon fiber reinforced thermoplastic composites based on induction heating which require the generation of eddy currents and therefore constrain the fiber orientations and stacking sequence. The framework is intended for inclusion in an MDO based aircraft wing weight estimation tool in which it is combined with aerodynamic analysis and optimization. Results obtained with the framework show the structural benefit of using variable stiffness also in case of multiple loadcases. The design variable formulation leads to acceptable calculation time while preserving accuracy and smoothness of the solution. Separation of optimizer and tow path planner allows multiple practical interpretations of the theoretical optimization result. This preserves the influence of the manufacturing engineer on the practical panel lay-up.

I. Introduction

The next level of performance of composite structures is likely to come from three major changes. First, the development of variable stiffness design and manufacturing principles. These will allow simultaneous design of load distribution and strength distribution. Although far from mature, there is significant evidence that variable stiffness structures will show unprecedented specific strength levels.[1,2,3,4,5,6] Figure 1 shows the world's first test on a computationally optimized variable stiffness panel with a row of cut-outs. The failure pattern shown by the panel indicated that variable stiffness enables fully stressed design and therefore very high structural efficiency. The panel shown failed at a load more than 50% higher than its constant stiffness equivalent.

*Professor, USC/McNAIR Center for Aerospace Innovation and Research, vantooren@cec.sc.edu, Senior Member.
†Postdoc Researcher, FPP Aerospace Engineering, A.Elham@tudelft.nl, Member.
‡Assistant Prof., USC/McNAIR Center, harik@mailbox.sc.edu.
§PhD Student, USC/McNAIR Center, uddinma@email.sc.edu.

Second, the development of fusion bonding based assembly of thermoplastic composites using induction, laser and ultrasonic heating principles. Figure 2 shows a recent and unique welded thermoplastic (constant stiffness) carbon composite control surface for a business jet.[7,8]

Third, the development of multi-polymer composite structures. Thermoset and thermoplastic polymers offer distinct advantages to the mechanical and manufacturing properties of a polymer composite material. It is advantageous to have zones of thermoplastic and zones of thermoset composite in a single structural element.[9]

To successfully combine these three developments, the scientific and engineering challenge is to design and create materials and structures for optimal performance taking into account requirements such as stiffness, strength, conductivity, thermal expansion, and the ability to be fusion bonded at selected zones. This requires a fundamental understanding of the multi-physical properties of variable stiffness, multi-polymer composite laminates and shells.

Figure 1. Failure of a variable stiffness panel loaded in tension. Note that failure is spread over the full panel instead of being concentrated at the edge of the cut-out. Courtesy Fokker Aerostructures BV, Delft University of Technology, CoDeT Engineering, NLR.

This paper focuses on the modeling and optimization part of fiber steering, a specialized version of automated fiber placement (AFP), to support the design of variable stiffness panels with cut-outs. While in normal AFP one tries to minimize non-geodesical placement of fibers in a part, fiber steering actually tries to utilize non-geodesical placement of fibers to control the load paths in the laminate as well as the laminate strength. Load path control is achieved by varying material stiffness w.r.t. a fixed coordinate system from point to point. The fundamental requirement to have displacement compatibility in a laminate is used to steer load to certain areas by making them stiffer. At the same time the strength of the laminate is influenced by the steering since strength of a laminate is directly related to the fiber directions in its constituing plies. Design for fiber steering therefore aims at the best match between loads and strength in each point of the laminate.

Figure 2. Induction welded thermoplastic composite business jet rudder.

AFP machines work with slit tapes also called tows. These tows are narrow, thin tapes of fiber based material. Each tow is typically 1/4 inch width, 0.25mm thick (including resin) for a typical $250gm/m^2$ base tape material and contains about 25-30k fibers. An AFP machine can lay-down several tows simultaneously in so-called courses. The design support tool discussed in this paper can help in defining courses of different numbers of tows. Tows have a finite width and different tow deformation mechanisms are required to put a tow flat on a non-planar surface. These mechanisms are not discussed in this paper, it is assumed that a minimum radius can be determined for a specific tow that assures adequate quality when the tow is used for in-plane steering based optimal design.

II. Basic Fiber Steering Design Problem

The design framework addresses the problem of finding the optimal fiber direction in each point P of each ply of a composite laminate with cut-outs loaded in plane stress. The plate problem under consideration defines a domain, Ω, bounded by multiple edges, Γ , in the $x-y$ reference plane, see figure 3. The state variables are the displacements in x and y direction, u and v respectively. The thickness of the plate, $h(x,y)$, is considered constant and small when compared to the plate dimensions in the $x-y$ plane.

The basic static equilibrium equations to be solved within the body are:

$$\frac{\partial \sigma_x}{\partial x} + \frac{\partial \tau_{xy}}{\partial y} + b_x = 0 \qquad \frac{\partial \tau_{xy}}{\partial x} + \frac{\partial \sigma_y}{\partial y} + b_y = 0 \tag{1}$$

And on the boundary by:

$$\sigma_x l + \tau_{xy} m = p_{xy} \qquad \tau_{xy} l + \sigma_y m = p_y \tag{2}$$

Here l and m are the directional $\sin\theta$ and $\cos\theta$ respectively. The plate is assumed to be a laminate consisting of one or more plies. Each ply can have a constant stiffness, i.e. independent from x, y or a variable stiffness, i.e. have a stiffness which is a function of x, y. The variation of the stiffness is assumed to be related only to variation of fiber directions in the ply.

The optimum direction for the fibers is defined as the minimum maximum failure index in all plies in all load cases. Constraints are formulated regarding minimum steering radius which is related to the tow properties. In addition plies can be specified to have a constant fiber direction with a predefined value.

The solution requires repeated analysis of the stress state, the calculation of all new fiber directions in the plate, the evaluation of the failure index in all elements and the evaluation of the manufacturing constraints. In the next section first the finite element model is described.

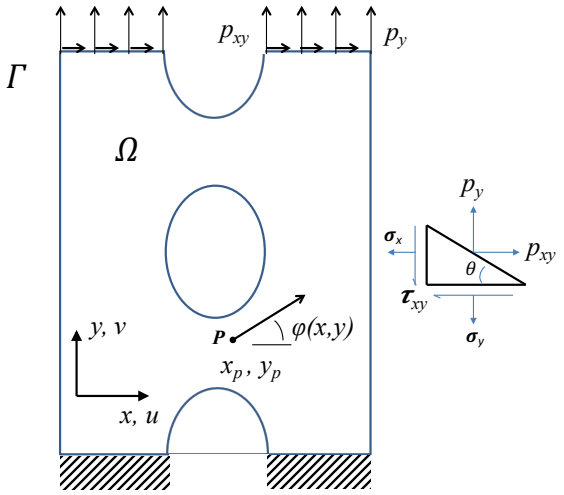

Figure 3. Basic geometry of the composite plate with cut-outs.

III. Finite Element Model

III.A. Kinematical Equations and Compatibility Conditions

The finite element model is based on 6-node, triangular quadratic elements using Lagrangian interpolation functions (shape functions), N_i^e, for the in-plane, membrane, displacements, u and v:

$$u = \sum_{i=1}^{n} N_i^e u_i \qquad v = \sum_{i=1}^{n} N_i^e v_i \tag{3}$$

In which u_i and v_i are the elements of the element's nodal displacement vector:

$$\mathbf{u}^e = \left\{ u_1 \quad v_1 \quad u_2 \quad v_2 \quad \cdots \quad \cdots \quad u_6 \quad v_6 \right\} \tag{4}$$

At this stage no out-of-plane deformation is taking into account. The triangular elements have three nodes at the vertices of the triangle and three nodes at the midpoints of the sides, see figure 4:

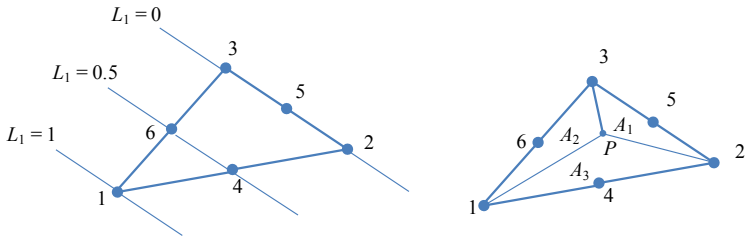

Figure 4. Node numbering and areal coordinates quadratic triangular element.

The interpolation functions are expressed in terms of area coordinates L_i:

$$L_i = \frac{A_i}{A}, A = \sum_{i=1}^{3} A_i \tag{5}$$

The definition of the area coordinates and an illustration of the values of L_1 within the element are given in figure 4. The Cartesian coordinates x and y can be expressed in terms of the area coordinates using:

$$\begin{aligned} x &= L_1 x_1 + L_2 x_2 + L_3 x_3 \\ y &= L_1 y_1 + L_2 y_2 + L_3 y_3 \\ 1 &= L_1 + L_2 + L_3 \end{aligned} \tag{6}$$

The Lagrange shape functions, N_i^e, which express the displacement in point x, y of element e related to the displacement in node i, are given by:

$$\begin{Bmatrix} N_1^e \\ N_2^2 \\ N_3^e \\ N_4^e \\ N_5^e \\ N_6^e \end{Bmatrix} = \begin{Bmatrix} L_1(2L_1-1) \\ L_2(2L_2-1) \\ L_3(2L_3-1) \\ 4L_1L_2 \\ 4L_2L_3 \\ 4L_3L_1 \end{Bmatrix} \tag{7}$$

This leads to the following approximation for the displacement field:

$$\mathbf{u} = \begin{Bmatrix} u(x,y) \\ v(x,y) \end{Bmatrix} = \begin{bmatrix} N_i^e & 0 & N_2^e & 0 & \cdots & N_6^e & 0 \\ 0 & N_1^e & 0 & N_2^e & \cdots & 0 & N_6^e \end{bmatrix} \mathbf{u}^e = N\mathbf{u}^e \tag{8}$$

Assuming linear relations between strains and displacements, the strain vector ξ can be derived from the displacement field $\mathbf{u}$ by derivation:

$$\xi = \begin{Bmatrix} \xi_x \\ \xi_y \\ \gamma_{xy} \end{Bmatrix} = \begin{Bmatrix} \frac{\partial u}{\partial x} \\ \frac{\partial v}{\partial y} \\ \frac{\partial u}{\partial y} + \frac{\partial v}{\partial x} \end{Bmatrix} = \begin{bmatrix} \frac{\partial N_1^e}{\partial x} & 0 & \frac{\partial N_2^e}{\partial x} & 0 & \cdots & \frac{\partial N_6^e}{\partial x} & 0 \\ 0 & \frac{\partial N_1^e}{\partial y} & 0 & \frac{\partial N_2^e}{\partial y} & \cdots & 0 & \frac{\partial N_6^e}{\partial y} \\ \frac{\partial N_1^e}{\partial y} & \frac{\partial N_1^e}{\partial x} & \frac{\partial N_2^e}{\partial y} & \frac{\partial N_2^e}{\partial x} & \cdots & \frac{\partial N_6^e}{\partial y} & \frac{\partial N_6^e}{\partial x} \end{bmatrix} = \mathbf{B}\mathbf{u}^e \tag{9}$$

Note that the derivatives in the matrix $\mathbf{B}$ are specified with respect to x and y while the shape functions are expressed in the natural coordinates L_i. Using partial differentiation we can write:

$$\frac{\partial N_i}{\partial L_j} = \frac{\partial N_i}{\partial x}\frac{\partial x}{\partial L_j} + \frac{\partial N_i}{\partial y}\frac{\partial y}{\partial L_j} \tag{10}$$

Performing the differentiation for all values of j and writing the result in matrix form yields:

$$\begin{Bmatrix} \frac{\partial N_i}{\partial L_1} \\ \frac{\partial N_i}{\partial L_2} \end{Bmatrix} = \begin{bmatrix} \frac{\partial x}{\partial L_1} & \frac{\partial y}{\partial L_1} \\ \frac{\partial x}{\partial L_2} & \frac{\partial y}{\partial L_2} \end{bmatrix} \begin{Bmatrix} \frac{\partial N_i}{\partial x} \\ \frac{\partial N_i}{\partial y} \end{Bmatrix} = \mathbf{J} \begin{Bmatrix} \frac{\partial N_i}{\partial x} \\ \frac{\partial N_i}{\partial y} \end{Bmatrix} \tag{11}$$

To find the global derivatives we invert $\mathbf{J}$ and write:

$$\begin{Bmatrix} \frac{\partial N_i}{\partial x} \\ \frac{\partial N_i}{\partial y} \end{Bmatrix} = \mathbf{J}^{-1} \begin{Bmatrix} \frac{\partial N_i}{\partial L_1} \\ \frac{\partial N_i}{\partial L_2} \end{Bmatrix} \tag{12}$$

$\mathbf{J}$ can easily be derived from the relation between the global coordinates x, y and the natural coordinates L_i, Eq. 6:

$$\mathbf{J} = \begin{bmatrix} \frac{\partial x}{\partial L_1} & \frac{\partial y}{\partial L_1} \\ \frac{\partial x}{\partial L_2} & \frac{\partial y}{\partial L_2} \end{bmatrix} = \begin{bmatrix} x_1 - x_3 & y_1 - y_3 \\ x_2 - x_3 & y_2 - y_3 \end{bmatrix} \tag{13}$$

The derivatives of the shape functions with respect to the natural coordinates can be derived from Eq. 7. For example:

$$\frac{\partial N_1}{\partial L_1} = \frac{\partial}{\partial L_1} L_1(2L_1 - 1) = 4L_1 - 1 \tag{14}$$

This leads to:

$$\begin{bmatrix} \frac{\partial N_i}{\partial L_j} \end{bmatrix}^T = \begin{bmatrix} 4L_1 - 1 & 0 & -3 + 4(L_1 + L_2) & 4L_2 & -4L_2 & 4 - 4L_2 - 8L_1 \\ 0 & 4L_2 - 1 & -3 + 4(L_1 + L_2) & 4L_1 & 4 - 4L_1 - 8L_2 & -4L_1 \end{bmatrix} \tag{15}$$

Multiplying this matrix with the inverse of $\mathbf{J}$ results in the required derivatives of the shape functions with respect to the global coordinates and subsequently the matrix $\mathbf{B}$, i.e. the kinematical relation. The compatibility condition is satisfied through Eq. 9.

III.B. Material Laws

Since we are considering a plane stress condition it is convenient to work with stress resultants:

$$N_x = \int_{-h/2}^{h/2} \sigma_x dz \qquad N_y = \int_{-h/2}^{h/2} \sigma_y dz \qquad N_{xy} = \int_{-h/2}^{h/2} \tau_{xy} dz \tag{16}$$

Since bending is not taken into account in this study, the stresses will be constant per layer k and the stress resultants can be simplified to:

$$N_x = \sum_{k=1}^{N} \sigma_x^{(k)} t_k \qquad N_y = \sum_{k=1}^{N} \sigma_y^{(k)} t_k \qquad N_{xy} = \sum_{k=1}^{N} \tau_{xy}^{(k)} t_k \tag{17}$$

Where t_k is the thickness of layer k. The relation between the plane-stress stress resultants and the strains for a laminated plate is given by the **A**-matrix defined by the Classical Laminate Theory (CLT):

$$\begin{Bmatrix} N_x \\ N_y \\ N_{xy} \end{Bmatrix} = \begin{bmatrix} A_{11} & A_{12} & A_{16} \\ A_{12} & A_{22} & A_{26} \\ A_{16} & A_{26} & A_{66} \end{bmatrix} \begin{Bmatrix} \xi_x \\ \xi_y \\ \gamma_{xy} \end{Bmatrix} \tag{18}$$

In which:

$$A_{ij} = \sum_{k=1}^{N} \left(\overline{Q}_{ij}\right)_k (z_k - z_{k-1}) \tag{19}$$

The coefficients $\left(\overline{Q}_{ij}\right)_k$ refer to the plane stress reduced stiffnesses of an orthotropic layer with its material axes oriented with an angle θ_k with respect to the laminate coordinates. The relation between the reduced stiffnesses of the base orthotropic layer $\left(Q_{ij}\right)_k$ and $\left(\overline{Q}_{ij}\right)_k$ is defined by:

$$\begin{aligned} \overline{Q}_{11} &= U_1 + U_2 \cos 2\theta_k + U_3 \cos 4\theta_k \\ \overline{Q}_{12} &= U_4 - U_3 \cos 4\theta_k \\ \overline{Q}_{21} &= U_1 - U_2 \cos 2\theta_k + U_3 \cos 4\theta_k \\ \overline{Q}_{16} &= (U_2 \sin 2\theta_k + 2U_3 \sin 4\theta_k)/2 \\ \overline{Q}_{26} &= (U_2 \sin 2\theta_k - 2U_3 \sin 4\theta_k)/2 \\ \overline{Q}_{66} &= U_5 - U_3 \cos 4\theta_k \end{aligned} \tag{20}$$

In which:

$$\begin{aligned} U_1 &= (3Q_{11} + 3Q_{22} + 2Q_{12} + 4Q_{66})/8 \\ U_2 &= (Q_{11} - Q_{22})/4 \\ U_3 &= (Q_{11} + Q_{22} - 2Q_{12} - 4Q_{66})/8 \\ U_4 &= (Q_{11} + Q_{22} + 6Q_{12} - 4Q_{66})/8 \\ U_5 &= (Q_{11} + Q_{22} - 2Q_{12} + 4Q_{66})/8 \end{aligned} \tag{21}$$

The coefficients $(Q_{ij})_k$ are known in terms of the engineering constants of the kth layer:

$$\begin{aligned} Q_{11} &= \frac{E_{11}}{1 - \nu_{12}\nu_{21}} \\ Q_{12} &= \frac{\nu_{12} E_{22}}{1 - \nu_{12}\nu_{21}} = \frac{\nu_{21} E_{11}}{1 - \nu_{12}\nu_{21}} \\ Q_{22} &= \frac{E_{22}}{1 - \nu_{12}\nu_{21}} \\ Q_{66} &= G_{12} \end{aligned} \tag{22}$$

Where E is the Young's modulus, ν the poisson ratio, and G the shear modulus.

III.C. Surface Forces and Boundary Conditions

The stress components on the boundary of the plate must be in equilibrium with the forces applied to this boundary, Eq. 2. If an external distributed load is assumed to work on the boundary defined by the edge of an element between node 1 and 2 (see figure 4), the shape functions can be used to express the load on the edge and find the nodal forces equivalent to the edge load. Since L_3 equals zero on this edge we have:

$$\mathbf{p} = \overline{p} \int \begin{bmatrix} L_1(2L_1 - 1) \\ L_2(2L_2 - 1) \\ 0 \\ 4L_1L_2 \\ 0 \\ 0 \end{bmatrix} ds \tag{23}$$

If we define the variable ξ as the variable describing the position on the edge and we take ξ_1 as the value at node 1 and ξ_2 as the value at node 2, the integral can be rewritten as:

$$\mathbf{p} = \overline{p} \int_{\xi_1}^{\xi_2} \begin{bmatrix} L_1(2L_1 - 1) \\ L_2(2L_2 - 1) \\ 0 \\ 4L_1L_2 \\ 0 \\ 0 \end{bmatrix} ds \tag{24}$$

Using the relation:

$$\begin{Bmatrix} L_1 \\ L_2 \end{Bmatrix} = \frac{1}{l_{12}} \begin{bmatrix} \xi_2 & -1 \\ -\xi_1 & 1 \end{bmatrix} \begin{Bmatrix} 1 \\ \xi \end{Bmatrix} \tag{25}$$

With l_{12} being the length of the edge defined by $\xi_2 - \xi_1$:

$$\mathbf{p} = \overline{p} \frac{l_{12}}{6} \begin{bmatrix} 1 & 1 & 0 & 4 & 0 & 0 \end{bmatrix}^T \tag{26}$$

III.D. Stiffness Matrix, Nodal Load and Equilibrium Equations

Combining the results from sections III.A, III.B, and III.C with the principle of virtual displacements, the stiffness matrix $\mathbf{K}$ and the nodal load vector $\mathbf{f}$ are found:

$$\mathbf{K}^e = \int_{\Omega^e} \mathbf{B}^T \mathbf{A} \mathbf{B} d\Omega^e \tag{27}$$

$$\mathbf{f}^e = \int_{\Gamma^e} N^T \hat{p} d\Gamma \tag{28}$$

The equilibrium equations for the element e can now be expressed as:

$$\mathbf{K}^e \mathbf{u}^e = \mathbf{f}^e \tag{29}$$

Integration over the full domain, i.e. all elements, leads to:

$$\mathbf{K}\mathbf{u} = \mathbf{f} \tag{30}$$

For the post-processing of the FE results the following equations are used to derive locals strains from displacements:

$$\begin{Bmatrix} \xi_x \\ \xi_y \\ \gamma_{xy} \end{Bmatrix} = \begin{Bmatrix} \xi_x \\ \xi_y \\ 2\xi_{xy} \end{Bmatrix} = \begin{Bmatrix} \frac{\partial u_0}{\partial x} \\ \frac{\partial v_0}{\partial y} \\ \frac{\partial u_0}{\partial y} + \frac{\partial v_0}{\partial x} \end{Bmatrix} = \sum_{j=1}^{m} \begin{Bmatrix} u_j \frac{\partial N_j^e}{\partial_x} \\ v_j \frac{\partial N_j^e}{\partial_y} \\ u_j \frac{\partial N_j^e}{\partial_y} + v_j \frac{\partial N_j^e}{\partial_x} \end{Bmatrix} \tag{31}$$

The stresses are derived from the strains with:

$$\begin{Bmatrix} \sigma_x \\ \sigma_y \\ \tau_{xy} \end{Bmatrix}^e = \begin{bmatrix} \overline{Q}_{11} & \overline{Q}_{12} & \overline{Q}_{16} \\ \overline{Q}_{12} & \overline{Q}_{22} & \overline{Q}_{26} \\ \overline{Q}_{16} & \overline{Q}_{26} & \overline{Q}_{66} \end{bmatrix}^e \left(\begin{Bmatrix} \xi_x \\ \xi_y \\ \gamma_{xy} \end{Bmatrix} - \begin{Bmatrix} \alpha_{xx} \\ \alpha_{yy} \\ 2\alpha_{xy} \end{Bmatrix} \Delta T \right) \tag{32}$$

Where α is the Coefficient of Thermal Expansion (CTE) and ΔT is the change in temperature.

III.E. Mesher

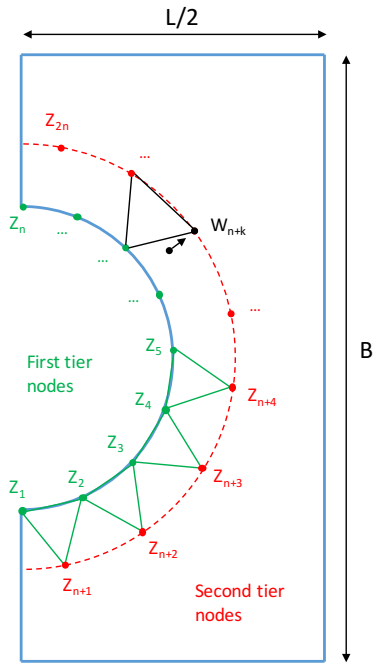

Figure 5. Generation of control mesh.

In order to facilitate the generation of mesh elements in a controlled and well-structured manner, the plate with dimensions $2L \times B$ is divided into three domains with lengths $L/2$, L, and $L/2$, respectively. The first and the last domains are mirror image of each other and can be mirrored and merged together to get the middle domain, which has a hole at the middle. Here, we develop an algorithm for generating mesh elements only at the middle domain, then copy appropriate parts of it on both sides to cover the first and the last domains. The overall mesh structure is then refined using a simple centroid adjustment process.

The mesh generation starts at the boundary of the central hole of the middle domain, which is discretized into a finite number of nodes (n), designated by complex number $Z = X + jY$. Here the origin (0,0) is at the center of the hole and (X, Y) are the coordinates on the periphery of the hole, which can be a circle, ellipse or a convex polygon with rounded corners. There will be a total of n nodes, from Z_1 to Z_n on the first tier of nodes. For any two consecutive nodes Z_1 and Z_2 on the edge of the hole, where a clockwise motion around the origin is required to go from Z_1 to Z_2,we get the third node Z_{n+1}, forming an equilateral triangle, see figure 5.

$$Z_{n+1} = \frac{Z_1 + Z_2}{2} + (Z_2 - Z_1)\sqrt{(\tfrac{-3}{4})} \tag{33}$$

Then Z_2 and Z_3 are used similarly to obtain:

$$Z_{n+2} = \frac{Z_2 + Z_3}{2} + (Z_3 - Z_2)\sqrt{(\tfrac{-3}{4})} \tag{34}$$

According to figure 5, (Z_1, Z_2, Z_{n+1}) and (Z_2, Z_3, Z_{n+2}) are the vertices of two equilateral triangles (elements) with Z_{n+1} and Z_{n+2} being nodes of the second tier. It is important to select the first tier nodes in the clockwise orientation to make sure that the second tier is not being formed inside the hole. Once the first two triangles are formed, (Z_{n+2}, Z_{n+1}, Z_2) are taken to be the vertices of another near-equilateral triangle filling the gap between the first two triangles. This process is repeated for all remaining first tier nodes, which results in exactly $2n$ elements being formed.

The second tier is formed with nodes Z_{n+1} to Z_{2n}, which are checked for concavity. Whenever a node goes outside of the boundary of the element domain, is it pinned to the nearest point on the boundary. For any node Z_{n+k} within the concave part of the second tier, a corrected node W_{n+k} is formed. An example is shown in figure 5:

$$W_{n+k} = \left[Z_{n+k} - \frac{Z_k + Z_{k+1}}{2} \right] h_k + \frac{Z_k + Z_{k+1}}{2} \tag{35}$$

$$Z_{n+k} = W_{n+k} \tag{36}$$

Where h_k is an empirical parameter obtained from the geometric orientation of the first two tiers that need not be unique for different implementation techniques. Once the second tier of nodes is fixed, the entire process is repeated for all subsequent tiers. Each tier adds n new nodes and $2n$ new elements, until any of the high level tiers intersects the boundary of the domain (dimensions $L \times B$). In such cases, the node Z_i, going outside the boundary of the domain, is fixed at the nearest point on the boundary. If all the

nodes on a tier require adjusting, this indicates total coverage of the domain with mesh elements. We then we look for all elements where all three nodes are on the same vertical or horizontal line and remove the element altogether; any of those three nodes not being shared by another valid element is also removed. This scenario happens due to the forcing of out-of-domain nodes on the boundary. Finding and removing such invalid nodes/elements at once is computationally more efficient than checking for such a situation during the formation of every single node/element.

After the elements are created in the middle domain (L×B), the right half of the middle domain is copied to the (L/2×B) domain on the left, and the left half of the middle domain is copied to the (L/2×B) domain on the right. This leads to exactly matching nodes on the boundary of adjacent domains. Any node that goes outside the boundary of the plate is pinned to the nearest point on the boundary, thus completely filling the plate with elements that are mostly well-shaped. Only the elements near the boundaries of each domain have irregular shapes due to the fact that many of them were forcefully pinned to the boundaries to prevent them from going off the boundaries. In order to refine such elements, a vertex adjustment process is used. This process takes every single node which is not on any boundary, finds its nearest neighbors, and shifts the node to the average of the vertices of the polygon formed by the said neighbors. For example, if Z_i is a node that is not on any physical boundary (this excludes the domain boundary within the plate), and is shared by six elements with nodes W_i (i = 1, 2, $\cdots$, 6) other than Z_i itself, then Z_i is defined by:

$$Z_i = \frac{\sum W_i}{6} \tag{37}$$

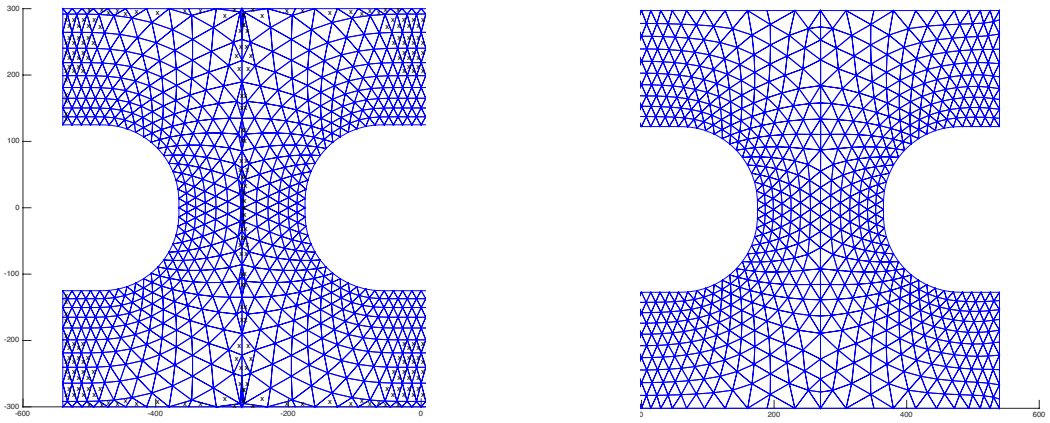

(a) Before. (b) After.

Figure 6. Symmetric left and right halves of the composite plate with cut-outs showing the FE mesh before and after refinement.

This simple process, after running iteratively for several cycles, significantly reduces the number of elements with irregular shapes, see figure 6. Even for the elements that cannot be refined fully by this process, angular irregularity (defined by the difference of the maximum angle and minimum angle of the element) is generally observed to be reduced. Finally, the middle point of each arm of each element is taken as another node, converting 3-node elements into 6-node elements for improved computational accuracy.

IV. Design Variable Definition

The intent of the tool is to find the optimum fiber directions in each point of the plate. The change of fiber direction from point to point means that the **A**-matrix in Eq. 27 is varying from element to element and even within each element. There are different approaches one could take to express the variation of the fiber directions in the stiffness matrix, Eq. 27. The use of lamination parameters has been reported as an effective way to parameterize the **A**-matrix.[10] This is, however, an indirect method since many lay-ups and fiber directions will lead to one and the same **A**-matrix. This approach therefore needs a postprocessing step to search for a best lay-up to achieve the optimal lamination parameter distribution. In the current study the fiber directions themselves have been used as the design variables.

The fiber direction distribution in a layer/ply can be seen as a scalar field. To control the field within the optimization the concept of a manufacturing mesh has been developed, see figure 7. A discretization of

the scalar field is obtained using a mesh of four node, rectangular elements. The elements have one degree of freedom per node, the fiber angle. Within each element the local fiber angle is defined using a set of four interpolation functions:

$$N_1 = \frac{1}{4ab}(x - x_2)(y - y_4) \qquad N_2 = \frac{1}{4ab}(x - x_1)(y - y_3) \tag{38}$$
$$N_3 = \frac{1}{4ab}(x - x_4)(y - y_2) \qquad N_4 = \frac{1}{4ab}(x - x_3)(y - y_1)$$

With:

$$a = (x_2 - x_1)/2 \qquad b = (y_4 - y_1)/2 \tag{39}$$

The fiber direction at point x, y in element e of ply k becomes:

$$\phi^{(e)} = \sum_{i=1}^{4} N_i^{(e)} \phi_i \tag{40}$$

In which ϕ_i are the values of the nodal fiber angles, i.e. the design variables.

In principle the discretization could have been done using the triangular elements used for the stress analysis. However, it was decided to separate the two since the stress mesh needs local refinement in areas with high stress gradients while the manufacturing mesh density is dictated by minimum allowable steering radius which is a constant for the complete domain. The number of elements in the manufacturing mesh is therefore much lower and the element size can be taken constant over the domain. To update the element stiffness matrices in each optimization step, the new nodal values of the fiber angles are used to calculate the fiber angle at the centroid of each stress element.

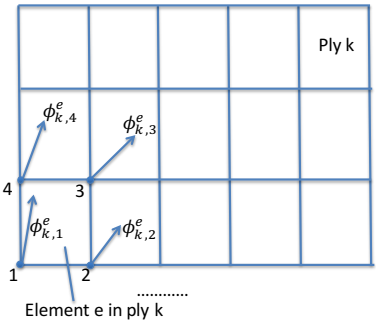

Figure 7. Manufacturing mesh. Each element e in ply k has four degrees of freedom: the nodal values of the fiber angles.

V. Objective Function and Constraint Functions

The objective function used for the optimization is the minimization of the maximum failure index in the plate. The failure index is evaluated at the centroid of each stress element. The Tsai-Hill failure criteria[11] is used to quantify the failure index:

$$FI = \frac{\sigma_x^2}{X^2} + \frac{\sigma_y^2}{Y^2} - \frac{\sigma_x \sigma_y}{XY} + \frac{\tau_{xy}^2}{S^2} \tag{41}$$

Here X and Y are the material strength in x, y direction respectively, S is the material shear strength. The constraints used during the optimization are the maximum allowed curvature, i.e. steering angle at the nodes. The curvature κ is evaluated at each node of the manufacturing mesh, in each element connected to that node with:

$$\kappa = \frac{d\phi}{ds} = \frac{\partial \phi}{\partial x}\frac{dx}{ds} + \frac{\partial \phi}{\partial y}\frac{dy}{ds} \tag{42}$$

With:

$$dx = ds \cos\phi \qquad dy = ds \sin\phi \tag{43}$$

The curvature can be expressed as

$$\kappa = \frac{d\phi}{ds} = \frac{\partial \phi}{\partial x}\cos\phi + \frac{\partial \phi}{\partial y}\sin\phi \tag{44}$$

With:

$$\frac{\partial \phi}{\partial x} = \sum_{i=1}^{4} \frac{\partial N_i}{\partial x}\phi_i \qquad \frac{\partial \phi}{\partial y} = \sum_{i=1}^{4} \frac{\partial N_i}{\partial y}\phi_i \tag{45}$$

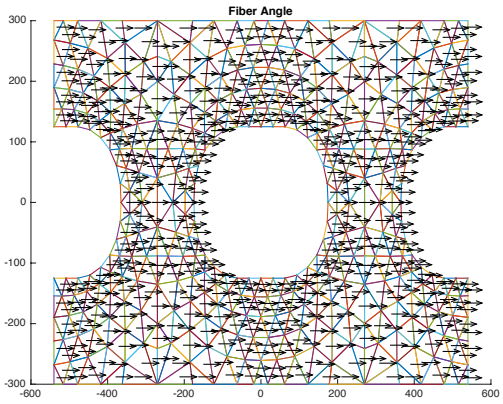

(a) Ply 3.

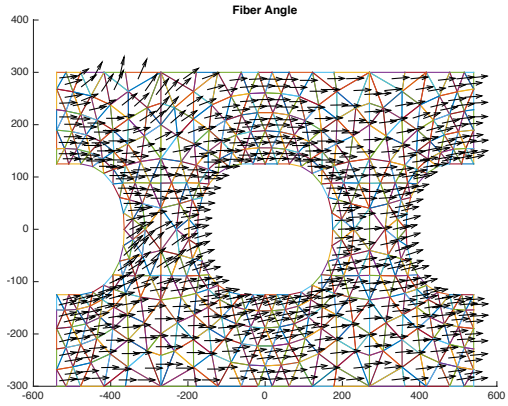

(b) Ply 3.

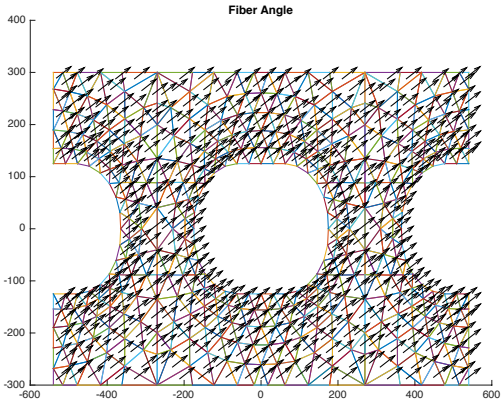

(c) Ply 4.

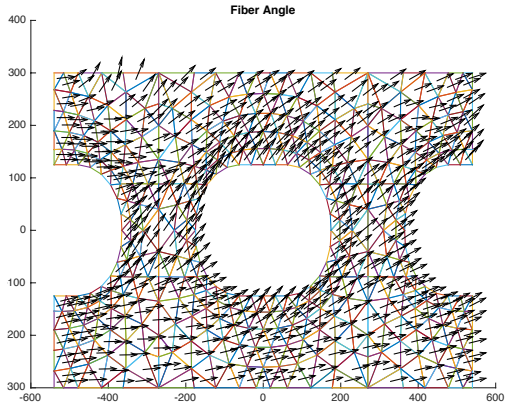

(d) Ply 4.

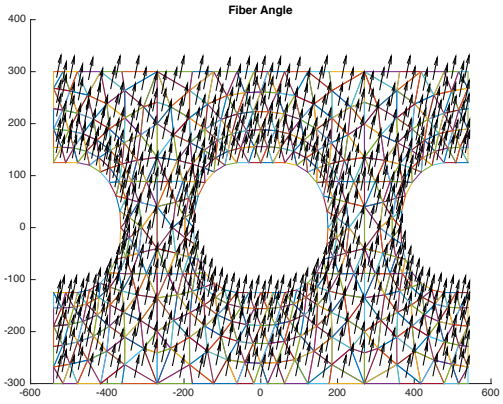

(e) Ply 5.

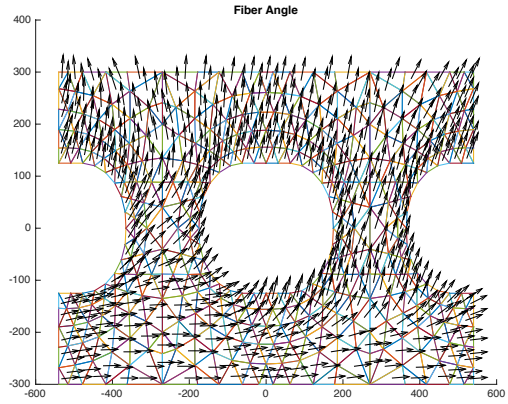

(f) Ply 5.

Figure 8. Fiber directions for plies 3-5, left column shows angles before and right column shows results after optimization.

VI. Implementation and Results

The FE module, the design variable definition and the objective and constraint functions have been implemented in a MATLAB[12] program. The stiffness matrix has been integrated exactly using the symbolic toolbox. The optimization toolbox has been used to find the optimal fiber directions at the nodes of the manufacturing mesh. In the figures below an example of the results is shown. The laminate being optimized consists of 10 plies, with the top and bottom two plies having a fixed fiber angle while the middle 6 plies are steered. Layer 6, 7 and 8 are mirrored versions of layer 3, 4 and 5 (i.e. angle in layer 6 is minus angle in layer 5) so only the nodal fiber angles of layer 3, 4 and 5 are required as design variables. Initial fiber directions for the 10 layers in degrees are [45, 135, 0, 30, 75, -75, -30, -0, 135, 45] w.r.t. the x-axis, counter-clockwise being positive.

The manufacturing mesh has 9x8 nodes, so the number of design variables is 216. The number of constraint functions is 224. Sequential Quadratic Programming is used as the optimizing method. The start and optimized fiber directions for ply 3, 4 and 5 are shown in figure 8.

The optimization process evolvement is shown in figure 9. It can be seen that the objective function, the maximum failure index in the plate, is reduced from an initial relative value of 1 to a value of 0.7.

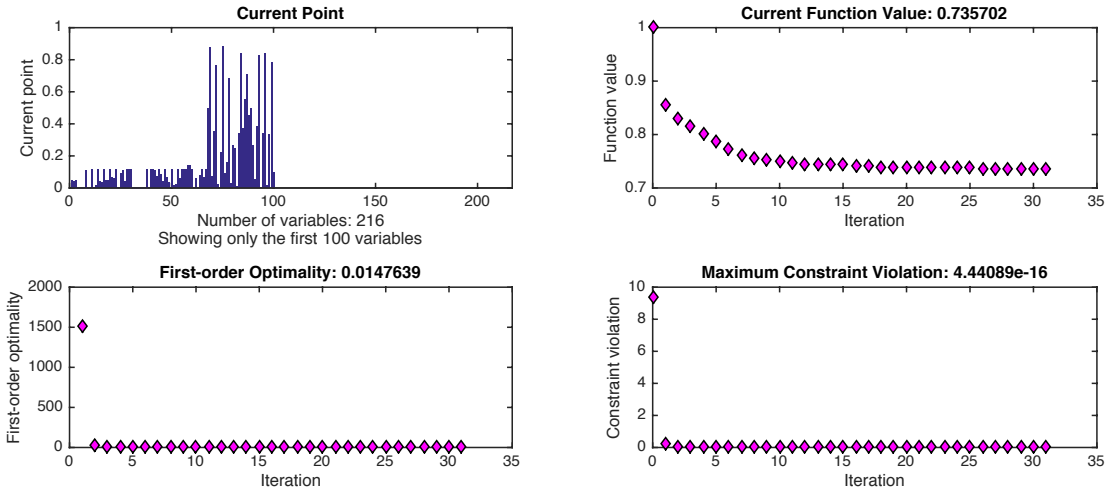

Figure 9. Evolvement optimization process with objective function value.

VII. Postprocessing the Results

VII.A. Methodology

Based on the fiber direction optimization results, the tow paths in each ply need to be generated. Since the optimized fiber directions are non-geodesical and change within each ply as a function of both x and y, i.e. the tow paths within each ply do not follow a pattern that leads to 100% coverage of the surface and a strategy needs to be selected for seeding starting points in each ply and for cutting and re-starting tows to create an acceptable level of coverage without too many overlaps and gaps.

A first approach for creating a tow planning seed mesh is presented here. The basic idea is to use a polygon positioned within the boundaries of the manufacturing mesh used for the ply under consideration, see figure 10. The line elements of the polygon are used to seed the tow paths. The most elementary implementation of the concept is using the four sides of the plate under consideration as the four sides of a polygon.

The concept relies on four different layered elements: laminate, manufacturing mesh, ply and polygon, see figure 10. The relation between those is: the laminate is the final product we try to define. It consists of plies. Each ply consists of a set of tows. The tow paths are calculated based on the fiber directions resulted from the optimization. These fiber directions are defined at this level based on the manufacturing mesh. The tow paths in an individual ply are calculated inside a polygon specific for the ply. The edges of the polygon are used to calculate initial points for the tow paths.

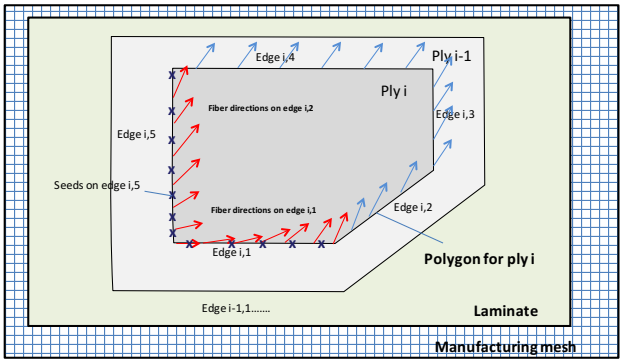

Figure 10. Tow path planning concept.

The tow path definition within a ply starts with the definition of the area within the ply that will be covered with tows. This area is defined using a polygon. The edges of the polygon are used to create the seeds for the tows. The basic formula used to calculate the seeds on each edge of the polygon is:

$$\mathbf{x}_{s,i+1} = \mathbf{x}_{s,i} + \frac{t_w + g_w}{|\sin(\theta_{f,i} - \theta_e)|}\mathbf{u}_e \quad \mathbf{x}_{s,i+1} < \mathbf{x}_{e,2} \tag{46}$$

Here t_w is the tow width and g_w is the gap width. There are however conditions in which this formula breaks down. The most often occurring failure condition is a very shallow angle between the fiber direction vector determined by $\theta_{f,i}$ and the edge direction vector determined by θ_e. The formula above will then lead to a very large step size, $\mathbf{x}_{s,i+1} - \mathbf{x}_{s,i}$. This means for the case shown below that only 1 seed point would be found on edge 1.

Currently this condition is handled through a limit on the step size in finding the next seed point based on a lower limit of $\theta_{f,i} - \theta_e$. This lower limit can be coupled to the minimum tow path radius which is a function of tow width and tow type. The minimum tow path radius is determined experimentally.

VII.B. Results

The methodology presented in section VII.A has been implemented in MATLAB.[12] The results are shown in figure 11.

VIII. Conclusion

The dual mesh approach presented in this paper for the optimization of fiber angles in a composite plate with cut-outs is effective in decoupling the discretization for stress calculations from the mesh used for the design variable definition. The interpolation functions used for the fiber angle calculation inside the elements of the manufacturing mesh based on the nodal values, i.e. the design variables, allow simple inclusion of the manufacturing constraints related to maximum allowable in-plane tow curvature. The presented tow path planner effectively translates the continuous distribution of optimizing fiber angles in each ply to discrete tows. The user can influence this translation by selection direction of path tracking and combining incoming and outgoing fiber paths. This allows manufacturing engineers and designers to incorporate practical considerations in the final design.

Acknowledgments

This research was partially supported by the Skolkovo Institute of Science and Technology (Skoltech), Russia.

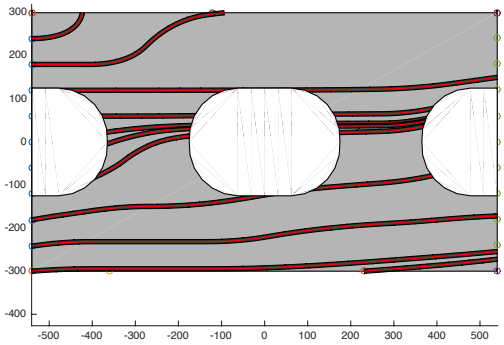

(a) Ply 3 fibers going in.

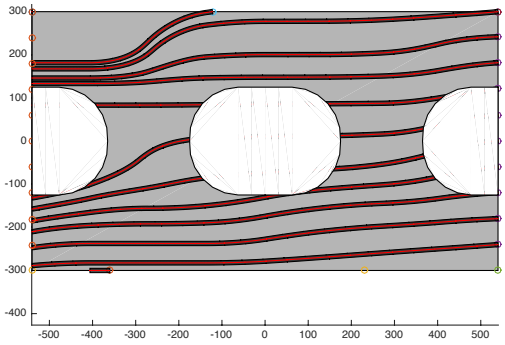

(b) Ply 3 fibers going out.

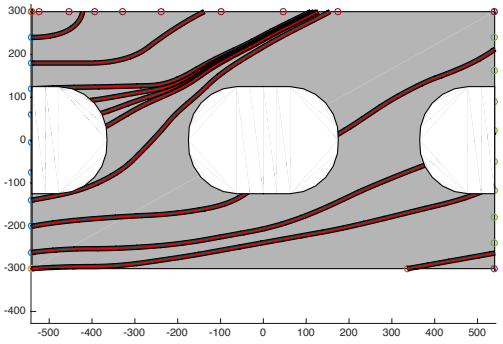

(c) Ply 4 fibers going in.

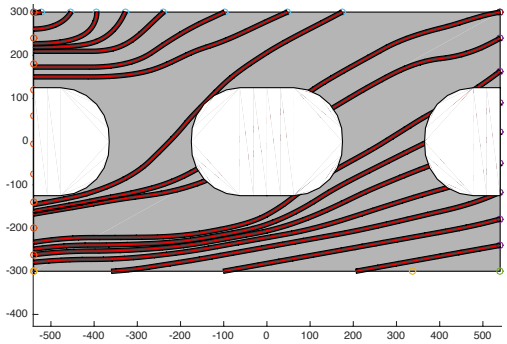

(d) Ply 4 fibers going out.

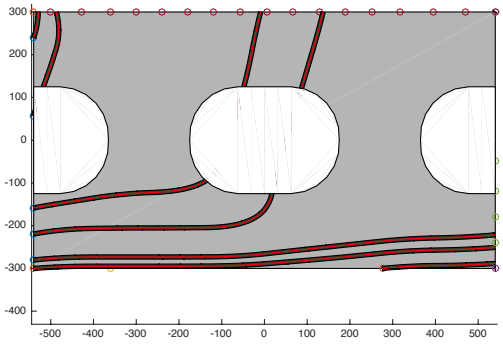

(e) Ply 5 fibers going in.

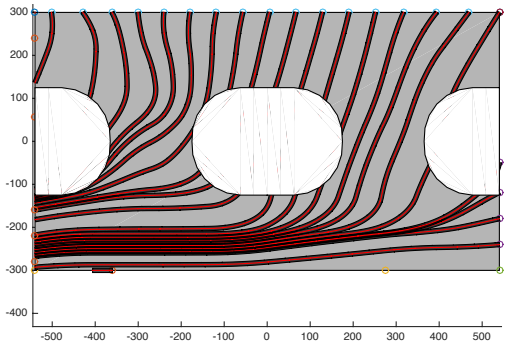

(f) Ply 5 fibers going out.

Figure 11. Tow placement plies 3 to 5 with seed points based on fibers going in and out.

References

[1]Wunderlich, W. and Pilkey, W. D., *Mechanics of Structures: Variational and Computational Methods*, CRC Press, Boca Raron (FL), 2nd ed., 2003.

[2]Krishnamoorthy, C., *Finite Element Analysis: Theory and Programming*, McGraw-Hill, Delhi, 1994.

[3]Reddy, J. N., *Mechanics of Laminated Composite Plates and Shells: Theory and Analysis*, CRC press, Boca Raron (FL), 2nd ed., 2004.

[4]Elham, A., van Tooren, M. J., and Sobieszczanski-Sobieski, J., "Bilevel Optimization Strategy for Aircraft Wing Design Using Parallel Computing," *AIAA Journal*, Vol. 52, No. 8, 2014, pp. 1770–1783.

[5]Gürdal, Z. and Zakhama, R., "Cellular Automata for Simultaneous Analysis and Optimal Structural Topology Design," *Simulating Complex Systems by Cellular Automata*, edited by J. Kroc, P. M. Sloot, and A. G. Hoekstra, Understanding Complex Systems, Springer Berlin Heidelberg, 1st ed., 2010, p. 350.

[6]Gürdal, Z., Abdelal, G., and Wu, K., "Experimental and Numerical Evaluation of Thermal Performance of Steered Fibre Composite Laminates," *Heat Transfer, Engineering Applications*, edited by V. Vikhrenko, InTech Open Access Publisher, Rijeka, Croatia, 2011, pp. 121–150.

[7]Koon, R., Engelstad, S. P., Tatting, B., and Gürdal, Z., "Highly tailored stiffening for advanced composites," March 1 2011, US Patent 7,897,239.

[8]Khani, A., Abdalla, M., and Gürdal, Z., "Circumferential stiffness tailoring of general cross section cylinders for maximum buckling load with strength constraints," *Composite Structures*, Vol. 94, No. 9, 2012, pp. 2851–2860.

[9]Van Campen, J. M., Kassapoglou, C., and Gürdal, Z., "Generating realistic laminate fiber angle distributions for optimal variable stiffness laminates," *Composites Part B: Engineering*, Vol. 43, No. 2, 2012, pp. 354–360.

[10]Setoodeh, S., Abdalla, M. M., and Gürdal, Z., "Design of variable–stiffness laminates using lamination parameters," *Composites Part B: Engineering*, Vol. 37, No. 4, 2006, pp. 301–309.

[11]Tsai, S. W., "Strength Characteristics of Composite Materials." Tech. rep., DTIC Document, 1965.

[12]MATLAB, *version 8.4 (R2014b)*, The MathWorks Inc., Natick, Massachusetts, 2014.